Combustion and Flame 158 (2011) 594–601

Contents lists available at ScienceDirect

Combustion and Flame

journal homepage: www.elsevier.com/locate/combustflame

The thermal dissociation/recombination reaction of hydrogen peroxide $H_2O_2(+M) \Longleftrightarrow 2OH(+M)$ III. Analysis and representation of the temperature and pressure dependence over wide ranges

J. Troe

Institut für Physikalische Chemie, Universität Göttingen, Tammannstrasse 6, D-37077 Göttingen, Germany
Max-Planck-Institut für biophysikalische Chemie, Am Fassberg 11, D-37077 Göttingen, Germany

ARTICLE INFO

Article history:
Received 24 June 2010
Received in revised form 10 August 2010
Accepted 26 August 2010
Available online 29 September 2010

Keywords:
H_2O_2 decomposition
OH recombination
Dissociation rates
Recombination rates

ABSTRACT

Experimental rate coefficients for the thermal dissociation $H_2O_2 + (M) \rightarrow 2OH(+M)$ and the reverse recombination $2OH(+M) \rightarrow H_2O_2(+M)$ are combined with recent modelling results based on an ab initio potential energy surface. The rate coefficients derived from the complementary experimental and modelling results are represented over wide ranges of temperature and pressure, such as being of interest for practical applications. Limiting low and high pressure rate coefficients as well as detailed and simplified expressions for rate coefficients in the falloff range are given.

1. Introduction

The thermal dissociation of hydrogen peroxide

$$H_2O_2(+M) \rightarrow 2OH(+M) \qquad (1)$$

plays an important role in the oxidation of hydrogen and hydrocarbons, see e.g. Refs. [1–7]. After formation of H_2O_2 in reactions like $HO_2 + H_2 \rightarrow H_2O_2 + H$ or $HO_2 + HO_2 \rightarrow H_2O_2 + O_2$, reaction (1) for instance contributes in an important way to the chain-branching at the third explosion limit of the hydrogen–oxygen system. With increasing interest in low temperature/high pressure combustion, not only the temperature but also the pressure dependence of reaction (1) finds renewed attention. This is the issue of the present article. It aims for a representation of the pressure and temperature dependence of reaction (1) and its reverse reaction

$$OH + OH(+M) \rightarrow H_2O_2(+M) \qquad (-1)$$

over wide ranges. It should be mentioned that reaction (−1) is also included in atmospheric chemistry models.

Reaction (1) has been studied frequently in the past, see e.g. Refs. [8–24], with most of the experiments performed near to the low pressure limit. Some deviations from limiting low pressure behaviour were noticed in Refs. [19,22]. Likewise, information on the pressure dependence came from studies of the recombination reaction (−1), see Refs. [25–31]. Theoretical work on the basis of an ab initio calculation of the potential energy surface [32] allowed one to establish the high pressure rate coefficient [33]. At the same time the latter has also been derived from pulse radiolysis experiments in liquid water [34] and quite satisfactory internal consistency between the high pressure rate coefficients has been observed. An alternative calculation of the high pressure rate coefficient, also on the basis of an ab initio potential, in Ref. [35] confirmed the results from Ref. [33]. In spite of the use of different theoretical methods, only marginal deviations were obtained which well illustrates the reliability of today's state of modelling.

The rate coefficients k_1 and k_{-1} have been evaluated several times for atmospheric and combustion chemistry, see e.g. Refs. [8–11]. In part, these evaluations were based on fragmentary or outdated information. The present article intends to provide a more updated analysis which combines the available experimental data with new theoretical results. In addition, a more updated link between k_1 and k_{-1} through the equilibrium constant will be provided than given in some of the reviews. The recommended rate coefficients then will be represented in compact form suitable for practical use.

2. Equilibrium constants

The rate coefficients k_1 and k_{-1} are linked by the equilibrium constant K_c through

E-mail address: shoff@gwdg.de

0010-2180/$ - see front matter © 2010 The Combustion Institute. Published by Elsevier Inc. All rights reserved.
doi:10.1016/j.combustflame.2010.08.013

$$K_c = k_1/k_{-1} \quad (2.1)$$

Relating experimental and theoretical results for k_1 and k_{-1} in an adequate and intrinsically consistent way thus requires proper care for the determination of K_c. While this statement sounds trivial, in practice it is not always fulfilled. For the present system, one major step was the revision of the heat of formation of OH radicals in Refs. [33–38]. This requires modifications of the tabulation of K_c such as presented, e.g. in Ref. [39], see below. It takes some time until such modifications are transferred into tabulations of kinetic data. Besides the revision in the heat of formation of OH, one also has to check the vibrational and rotational contributions to K_c such as used in compilations like Refs. [39,40]. This can be done by making use of recent spectroscopic studies. By now, the reaction enthalpy at 0 K for reaction (1) of ΔH^o (0 K)/R = 24,532 (±30) K from the "Active Thermochemical Tables" of Ref. [35] agrees with the more precise value of ΔH^o (0 K)/R = 24,534 (±6) K which was obtained earlier in the spectroscopic work of Ref. [41].

In order to illustrate the relevance of various revisions on the values of K_c, in Table 1 we compare data from various sources obtained at various stages. Part of the differences are due to different values of ΔH, part are due to different treatments of the hindered internal rotor/torsional oscillator of H_2O_2, and part are caused by the use of simplified fit expressions for K_c. In the present work we employ values for K_c which were calculated in Ref. [33] on the basis of the spectroscopic determination of ΔH and the torsional levels of H_2O_2 [42,43]. Over the range 500–1000 K, in which experimental results for recombination and dissociation are available, these results are fitted in the form

$$K_c = 71.4(T/1000\ \mathrm{K})^{1.1} \exp(-24,534\ \mathrm{K}/T)\ \mathrm{mol\ cm^{-3}} \quad (2.2)$$

Over the range 1000–1500 K, on the other hand, the results are fitted by

$$K_c = 71.4(T/1000\ \mathrm{K})^{0.25} \exp(-24,534\ \mathrm{K}/T)\ \mathrm{mol\ cm^{-3}} \quad (2.3)$$

Table 1 illustrates the respective deviations of K_c from the values preferred here. They span a factor of 1.8 at 500 K, 1.3 at 1000 K, and 1.2 at 1500 K.

3. Modelling of rate coefficients

In view of the fact that experimental data for the temperature and pressure dependences of k_1 and k_{-1} are fragmentary and that the theoretical modelling on the basis of ab initio potential data is on a comparably firm ground we first present modelled strong collision falloff curves. We then compare these with experimental results. This comparison, first, illustrates the degree of internal consistency of the experimental data, and of experiment with modelling. Second, the unknown collision efficiencies β_c and the related average energies for collisional energy transfer $\langle\Delta E\rangle$ are fitted. From other experiments one knows which values are "reasonable", but β_c and $\langle\Delta E\rangle$ unavoidably still remain fit parameters. Some ambiguity also is given by the proper choice of the appropriate collision frequency Z, see Refs. [44,45]. Third, we look for evidence for deviations from statistical reaction behaviour, see Ref. [33].

Table 1
Equilibrium constants K_c (in mol cm^{-3}) from various sources.

	T/K		
Reference	500	1000	1500
JANAF [39]	1.31×10^{-20}	1.39×10^{-9}	5.46×10^{-6}
GRI-Mech 3.0 [9]	1.00×10^{-20}	1.24×10^{-9}	5.18×10^{-6}
JANAF (scaled)[a]	2.45×10^{-20}	1.90×10^{-9}	6.73×10^{-6}
IUPAC [10],[b]	2.90×10^{-20}	1.93×10^{-9}	6.48×10^{-6}
This work[c]	1.64×10^{-20}	1.58×10^{-9}	6.23×10^{-6}

[a] Values from Ref. [39] scaled accounting for revised ΔH from Refs. [36–38], i.e. data of Ref. [39] multiplied by exp(−315 K/T).
[b] Data from Ref. [40] scaled with revised ΔH from Refs. [36,37], results represented in the form $K_c = 4.23 \times 10^5\ T^{-1.066}$ exp(−25,660 K/T) mol cm^{-3} over the range 300–500 K.
[c] Calculations from Ref. [33] and the present work, based on spectroscopic molecular parameters from Refs. [32,41–43], results represented in the form of Eqs. (2.2) and (2.3)).

3.1. High pressure rate coefficients

In the work of Ref. [33], the limiting high pressure rate coefficients $k_{-1,\infty}$ for the recombination (−1) was calculated by the statistical adiabatic channel model/classical trajectories (SACM/CT) method employing the ab initio potential from Ref. [32]. Over the range 60–5000 K, the results could be fitted by the expression

$$\begin{aligned} k_{-1,\infty} &= [2.26(298\ \mathrm{K}/T)^{0.47} + 0.0783(T/298\ \mathrm{K})^{0.74}] \\ &\quad \times 10^{13}\ \mathrm{cm^3\ mol^{-1}\ s^{-1}} \\ &= [0.376(298\ \mathrm{K}/T)^{0.47} + 0.013(T/298\ \mathrm{K})^{0.74}] \\ &\quad \times 10^{-10}\ \mathrm{cm^3\ molecule^{-1}\ s^{-1}} \end{aligned} \quad (3.1)$$

We consider this value considerably more reliable than the extrapolated experimental values, while we note the consistency with the experimental data from Refs. [30,31,34] (see also below). Eq. (3.1), therefore, is used unchanged. The modelling results of Ref. [33], such as represented by Eq. (3.1), near room temperature agree very well with the results of Ref. [35], while they exceed some of the latter results by 20–30% near 1500 K. However, the various models employed in Ref. [35] also led to a similar spread of results such that this difference appears to be of no major relevance. One finally should also note the very good agreement of the results from Refs. [33,35] with a modelling mentioned in Ref. [46] which made use of one of the methods employed in Ref. [35]. One, therefore, may estimate the uncertainty of the modelled $k_{-1,\infty}$ to be of the order of ±20%, i.e. being much smaller than that of extrapolated experimental results, see below.

3.2. Low pressure strong collision rate coefficients

We model the limiting low pressure strong collision rate coefficients $k_{1,0}^{SC}$ following the method described in Refs. [47–49]. The various factors entering into $k_{1,0}^{SC}$ are briefly summarized in the following.

Vibrational partition functions Q_{vib} of H_2O_2 and OH are calculated with the fundamental frequencies and torsional/hindered internal rotor levels of H_2O_2 given in Refs. [32,33,41–43]. The anharmonic vibrational density of states $\rho_{vib,h}(E_0)F_{anh}$ at the dissociation energy E_0 was calculated independently in Ref. [50]. At E_0/hc = 17,052 cm^{-1}, $\rho_{vib,h}(E_0)F_{anh}$ = 19.0 per cm^{-1} was obtained. In calculating Q_{vib} and $\rho_{vib,h}(E_0)F_{anh}$ for H_2O_2, the inversion doubling has to be accounted for. For Q_{vib}, all A^+ and A^- energy levels were explicitly included in the torsional partition function which was separated from the contribution of the remaining five oscillators treated in harmonic approximation. $\rho_{vib,h}(E_0)F_{anh}$ was the smoothed derivative of the number of levels $W(E, J = 0)$ such as obtained by quantum-corrected Monte Carlo calculation of the phase space volume on the ab initio potential, see Ref. [50] (note that Eq. (5.1) for $W(E, J = 0)$ of Ref. [50] corresponds to the average of A^+ and A^- levels and thus represents $W(E, J = 0)/2$. If a harmonic torsional frequency of 170 cm^{-1} is chosen in order to reproduce the correct $W(E, J = 0)$ at low energies and all A^+ and A^- levels are included, then F_{anh} = 1.64 from Eq. (5.2) is consistent with $W(E, J = 0)$ from Eq. (5.1) of Ref. [50]).

Rotational factors $F_{rot}(T)$ were determined in Ref. [33] by making use of the explicit representation of centrifugal barriers

$E_0(J)$ determined for the ab initio potential. The factor F_E accounting for the energy dependence of the vibrational density of states was also determined. The results from Ref. [33] are $(F_{rot}, F_E) = (98.4, 1.03), (56.2, 1.05), (37.6, 1.07), (27.4, 1.09), (21.1, 1.10), (17.1, 1.12), (14.1, 1.14), (12.0, 1.16), (10.3, 1.18), (9.03, 1.20), (7.98, 1.22), (7.13, 1.24), (6.42, 1.26)$, and $(5.82, 1.29)$ for $T = 200, 300, 400, \ldots, 1500$ K, respectively.

When collision frequencies Z are expressed by the Lennard–Jones frequencies Z_{LJ}, Lennard–Jones parameters σ and ε from Refs. [51,52] may be chosen. They are $(\sigma/\text{Å}, (\varepsilon/k)/\text{K}) = (4.196, 289.3), (2.551, 10.22), (3.542, 93.3), (3.798, 71.4), (3.467, 106.7), (3.941, 195.2)$, and $(2.641, 809.1)$, for H_2O_2, He, Ar, N_2, O_2, CO_2, and H_2O, respectively. While Z_{LJ} represents a convenient reference collision frequency, it may not necessarily be appropriate if reactant and buffer gas M have permanent dipole moments. We have considered this situation for the recombination $H + O_2 + M \rightarrow HO_2 + M$ in Ref. [45] and discussed alternative options for Z, such as given by dipole-induced dipole or dipole–dipole capture rate constants (Z_{d-id} or Z_{d-d}, respectively) from Ref. [53]. It was found that Z_{d-id} and Z_{d-d} were about a factor of 1.8 (±0.1) larger than Z_{LJ}. We do not repeat such investigations for the present system, but keep in mind this option which leads to different apparent values of β_c and $\langle\Delta E\rangle$ from the analysis of experimental data.

The results of our modelling of limiting low pressure dissociation rate coefficients $k_{1,0}$ are expressed by the calculated ratio $k_{1,0}/\beta_c Z[\text{M}]\exp(-E_0/\text{kT})$. We obtained the values $(8.81, 6.92, 5.57, 4.52, 3.67, 2.99, 2.44, 2.00, 1.65, 1.36, 1.13, 0.946, 0.794, 0.669) \times 10^4$, for $T = 200, 300, 400, \ldots, 1500$ K, respectively. The results for our limiting low pressure strong collision recombination rate coefficients $k_{-1,0}$ are expressed by the ratio $k_{-1,0}/\beta_c Z[\text{M}]$. Here, we obtained the values $(17.4, 5.48, 2.48, 1.36, 0.844, 0.567, 0.405, 0.301, 0.232, 0.183, 0.147, 0.122, 0.101, 0.0846) \times 10^4$ cm^3 mol^{-1}, for $T = 200, 300, 400, \ldots, 1500$ K, respectively.

3.3. Falloff curves

SACM/CT calculations of the specific rate constants $k(E, J)$ for H_2O_2 dissociation in Ref. [33] have been performed employing the ab initio potential from Ref. [32]. By means of these $k(E, J)$, strong collision falloff curves for H_2O_2 dissociation and recombination were calculated in Ref. [33]. These falloff curves to some extent differ from the "standard form" [49,54–56]

$$k/k_\infty = [x/(1+x)]\,F(x) \tag{3.2}$$

where

$$F(x) = F_c^{\{1+[\log x/\text{N}]^2\}^{-1}} \tag{3.3}$$

with $x = k_0/k_\infty$ and $N \approx 0.75–1.27 \log F_c$ (k stands for k_1 and k_{-1}). The strong collision broadening factors $F(x)$ in Refs. [49,54–56] were found to be asymmetric relative to $\log x = 0$ and the minimum was shifted towards x-values smaller than unity. Such deviations from Eq. (3.3) were tentatively represented in the form [49,54–56]

$$F(x) = F_c^{\{1+[(c+\log x)/(N+\Delta N)]^2\}^{-1}} \tag{3.4}$$

with c being of the order of 0.1 to −0.3 and ΔN of the order of $\pm[0.1 + 0.6 \log F_c]$, with the positive sign for $(c + \log x) > 0$ and the negative sign for $(c + \log x) < 0$. This leads to falloff curves which are broader at the low pressure side than on the high pressure side. In addition to the asymmetries of the strong collision falloff curves, weak collision broadening of the curves has to be accounted for. Systematic solutions of the master equation in Refs. [49,54] suggested that, to a first approximation, this can be done by representing F_c in Eqs. (3.4) and (3.5) by the product of strong collision and weak collision center broadening factors F_c^{SC} and F_c^{WC} respectively, where F_c^{WC} is roughly related to the collision efficiency β_c through

$$F_c^{WC} \approx \beta_c^{0.14} \tag{3.5}$$

For $\beta_c < 0.1$,

$$F_c^{WC} \approx 0.58\beta_c^{0.2} + 0.42 \tag{3.6}$$

in Ref. [57] was found to be more appropriate. Although this is only a temporary solution of the problem and more detailed solutions of the master equation are necessary when, besides $k(E, J)$, also rovibrational energy transfer is better understood, Eqs. (3.5) and (3.6) at the present stage may serve as a guide.

The strong collision falloff curves with the detailed calculations for H_2O_2 from Ref. [33] can be represented only approximately by Eqs. (3.3) and (3.4). In view of the mentioned uncertainties in the weak collision broadening factors, however, we abstain from modifying Eq. (3.4) for better agreement with the detailed strong collision results from Ref. [33]. Instead, we force these results to the form of Eq. (3.4). In this case, the strong collision center broadening factors are fitted by

$$F_c^{SC} \approx 1 - 0.5\exp[-(T - 200\ \text{K})/3700\ \text{K}] \tag{3.7}$$

while $N^{SC} \approx 0.75–1.27 \log F_c^{SC}$, $\Delta N^{SC} \approx 0.22\ N^{SC}$, and $c^{SC} \approx 0.2$ are the corresponding strong collision parameters in Eq. (3.4). Figure 1, for 300 K, compares modelled strong collision broadening factors from Eqs. (3.2) and (3.4), employing these parameters, with the calculated detailed results. The agreement looks satisfactory over the low pressure half of the curve ($x < 0.2$) while larger deviations are observed in the high pressure part ($x > 1$).

In practical applications, weak collision center broadening factors F_c^{WC} are estimated through Eqs. (3.5) and (3.6) from collision efficiencies β_c such as determined from the analysis of experimental low pressure rate coefficients. Then, $F_c = F_c^{SC}F_c^{WC}$ serves for the estimate of joint parameters N, ΔN, and c through $N \approx 0.75–1.27 \log F_c$, $\Delta N \approx 0.22$ N, and $c \approx 0.2$, to be used in Eqs. (3.2) and (3.4). Figure 1 indicates that rate coefficients represented in the simplified form of Eqs. (3.2)–(3.4) do not differ from detailed modelling results by more than about 10%. When higher precision would really be required, then the graphical representation of the detailed modelling results from Ref. [33], i.e. curve 1 from Fig. 1, should be employed. However, at the same time a more detailed account for weak collision effects in terms of realistic rovibrational energy transfer would have to be made.

One final remark concerns the temperature dependence of the broadening factors. The strong collision center broadening factors F_c^{SC}, for the present system at $T > 200$ K, increase with increasing temperature such as documented also in Ref. [55]. On the other hand, collision efficiencies β_c decrease such that F_c^{WC} also decreases with increasing temperature. As a consequence of these two counteracting trends, nearly temperature independent center broadening factors $F_c = F_c^{SC}F_c^{WC}$ provide a practically acceptable first approximation (at least for inefficient colliders; for strong colliders, Eq. (3.7) should be used).

4. Combination of experimental and modelled rate coefficients

4.1. Recombination experiments

The recombination reaction (−1) has been studied from about 200 to 700 K, whereas results for the dissociation (1) were obtained over the range 650–1450 K. Experiments intended to measure recombination rate coefficients k_{-1} were performed over a pressure range from about 0.05 to 150 bar whereas k_1 was determined over the range from about 3×10^{-4} to 20 bar. Although these pressure ranges appear impressively large, a look at modelled falloff curves

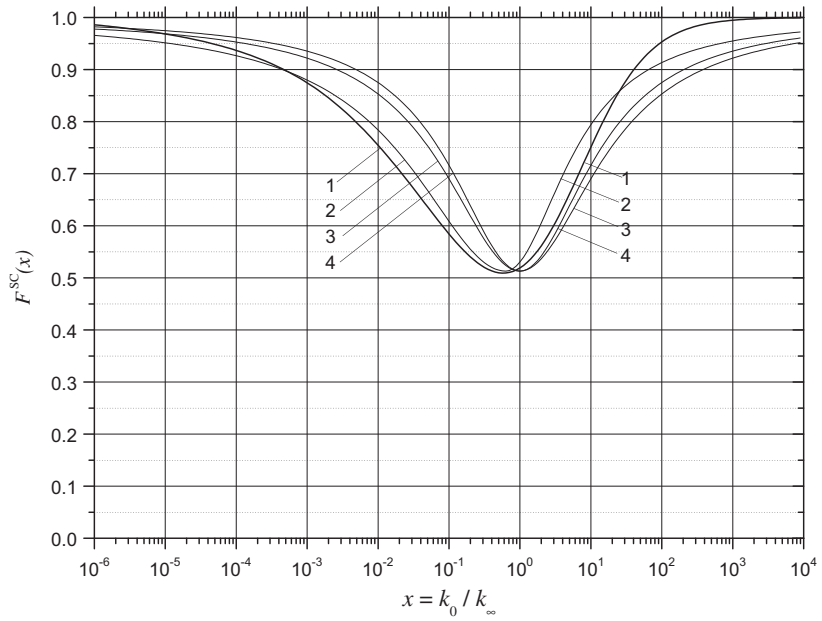

Fig. 1. Strong collision broadening factors $F^{SC}(x)$ at 300 K (curve 1: detailed modelling from Ref. [33]; curve 2: simplified representation by Eq. (3.4) with $F_c = 0.513$, $c = 0.2$, $N = 1.118$, and $\Delta N = 0.246$; curve 3: simplified representation by Eq. (3.3) with $F_c = 0.513$ and $N = 1.118$; curve 4: simplified representation by Eq. (3.2) with $F_c = 0.513$, see text).

such as shown in Figs. 1–3 clearly indicates that only minor parts of the falloff curves were accessible in this way and that limiting rate coefficients could not have been attained to better than 10%. Complete falloff curves thus cannot be constructed without combining experimental and modelled rate coefficients. The collision efficiency β_c and the corresponding average energy $\langle\Delta E\rangle$ transferred per collision remain fit parameters. A simplification is obtained, if one assumes that $\langle\Delta E\rangle$ (including up- and down-collisions) depends only weakly on the temperature (see, e.g. Refs. [4,52]).

We demonstrate the construction of a complete falloff curve for recombination near 300 K. Early low temperature measurements [25,26] of k_{-1} apparently had problems [27] with the calibration of OH signals such that the absolute values of the derived rate

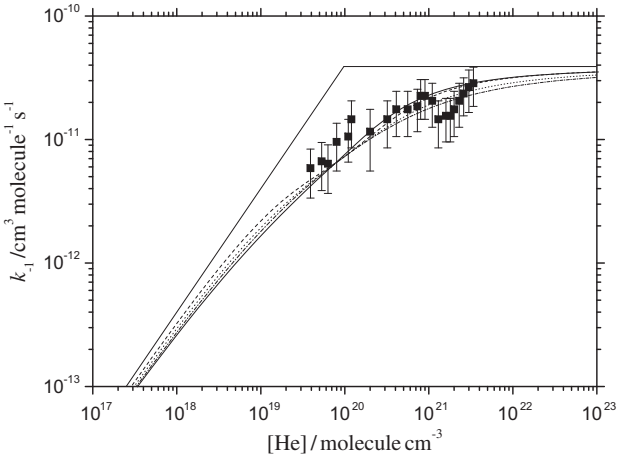

Fig. 2. Experimental recombination rate coefficients k_{-1} and their modelled falloff representation (M = He and $T = 300$ K; = experimental points from Ref. [30]; full lines = modelled limiting low and high pressure rate coefficients of this work with $k_{-1,0} = [\mathrm{He}]\ \ 0.4 \times 10^{-30}$ cm^6 molecule^{-2} s^{-1} and $k_{-1,\infty} = 3.9 \times 10^{-11}$ cm^3 molecule^{-1} s^{-1}; dashed line = representation by Eq. (3.2) with $F_c = 0.37$; dotted line = representation by Eq. (3.3) with $F_c = 0.37$ and $N = 1.30$; dash-dotted line = representation by Eq. (3.3) with $F_c = 0.37$ and $N = 1.52$; full line = representation by Eq. (3.4) with $F_c = 0.37$, $N = 1.30$, $\Delta N = 0.22$, and $c = 0.2$, see text).

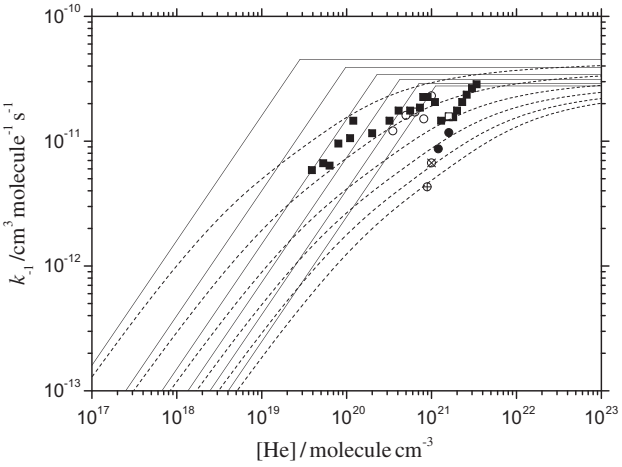

Fig. 3. Experimental recombination rate coefficients k_{-1} and their modelled falloff representation (M = He, experimental points from Refs. [30,31] at $T/K = 210$ (○), 298 (■), 406 (□), 510 (●), 614 (⊗), and 694 (⊕); full lines = modelled limiting low and high pressure rate coefficients from Section 5 of this work; dashed lines = falloff representation by Eq. (3.3) with $F_c = 0.37$ and $N = 1.32$).

coefficients remained uncertain. The later measurements of Refs. [27–31] overcame this problem by measuring absolute OH concentrations. These studies are considered in the following. The earliest two of these studies [27,28] recognized the importance of mechanistic complications of the experiments. Besides reaction (−1), the sequence

$$\mathrm{OH} + \mathrm{OH} \rightarrow \mathrm{H_2O} + \mathrm{O}(^3\mathrm{P}) \qquad (2)$$

which takes place on a triplet potential surface [58] in contrast to the singlet potential of H_2O_2 of reactions (1) and (−1),

$$\mathrm{O} + \mathrm{OH} \rightarrow \mathrm{O_2} + \mathrm{H} \qquad (3)$$

and

$$H + OH(+M) \rightarrow H_2O + M \quad (4)$$

were considered. As a consequence, the observed OH profiles were determined by plotting $[OH]^{-1} = [OH]_{t=0}^{-1} + k_{eff}t$ against time t where

$$k_{eff} = 2k_{-1}[M] + 3k_2 + k_4[M] \quad (4.1)$$

The determination of k_{-1}, thus, depended on knowing of the values for k_2 and k_4. k_2 was derived in Refs. [27,28], but since then has slightly been modified [10,11,59–61] and is now well established as $k_2 = 4.3\ (\pm 0.6) \times 10^{11}\ \exp(210\ K/T)\ cm^3\ mol^{-1}\ s^{-1}$ over the range 230–360 K [59] and $k_2 = 9.4 \times 10^{-5}\ T^{4.77}\ \exp(4570\ K/T)\ cm^3\ mol^{-1}\ s^{-1}$ over the range 1050–2380 K [57]. For the bath gas M = N_2, $k_4 = 6.1 \times 10^{-26}\ T^{2.0}\ cm^6\ molecule^{-2}\ s^{-1}$ was recommended in Ref. [10] with an uncertainty of about a factor of three near 300 K. Inserting these values for k_2 and k_4 into Eq. (4.1), one realizes that near room temperature k_{-1} only contributes to a small extent to k_{eff}. As a consequence, the difference by a factor of 2 between the derived values for k_{-1} from Refs. [27,28] is not surprising. Using the now preferred value for k_2 from Ref. [59] and employing k_4 as given above, one even comes to the conclusion that k_{-1} with M = N_2 neither in Ref. [27] nor in Ref. [28] could be identified at all. Similar arguments apply to the less extensive studies with M = SF_6 from Ref. [29]. Although more or less realistic values for k_{-1} in Refs. [27,28] were obtained, this fact has to be considered as accidental. The data of these references thus should not further be taken into account.

The problem with secondary reactions in OH recombination studies was only overcome in Refs. [30,31] when O atoms from reaction (2) were intercepted by added excess O_2, forming O_3 which only slowly further reacts with OH. Therefore, in the following we only consider the measurements of k_{-1} from Refs. [30,31]. We note that only M = He was used in these studies. Subtracting k_2 from $k_{-1,exp}$ of Refs. [30,31], the experimental results are illustrated in Figs. 2 and 3. One realizes that these experiments were all done in the middle part of the falloff curve. Together with the modelled value of the high pressure limiting rate coefficients $k_{-1,\infty}$ from Section 3, one may try to obtain the low pressure limiting rate coefficient $k_{-1,0}$ by extrapolation. Even the most extensive measurements near 300 K from Fig. 2 allow this to be done only with a factor of three uncertainty. Nevertheless, combining the derived value with the strong collision modelling of Section 3, one obtains a collision efficiency of $\beta_c \approx 0.1$ at 300 K which corresponds to $-\langle\Delta E\rangle/hc \approx 32\ cm^{-1}$. Although larger than the value of 5.5 cm^{-1}, derived for the reaction H + O_2 + He → HO_2 + He in Ref. [45], the result for the four atomic H_2O_2-system appears not unreasonable. It may already be noted at this stage that the value of $\langle\Delta E\rangle$, derived only semiquantitatively from the falloff curve of Fig. 2, agrees well with values obtained from dissociation experiments such as analyzed below. Provided that $\langle\Delta E\rangle$ is only weakly temperature dependent, the recombination and dissociation experiments in M = He thus are consistent with each other.

The results of Fig. 2 can be represented in various ways, essentially being indistinguishable within the experimental uncertainty. The collision efficiency $\beta_c \approx 0.1$ at 300 K with Eq. (3.5) leads to $F_c^{WC} \approx 0.72$. Combining this with F_c^{SC} from Eq. (3.7) and assuming T-independent $\langle\Delta E\rangle$ leads to a nearly temperature independent center broadening factor of $F_c \approx 0.37$ between 300 and 700 K. Falloff curves for such low F_c, using $F(x)$ of Eq. (3.3) with $N = 1$, are known to show small "wiggles" such as also illustrated in Fig. 2. When $N = 0.75–1.27 \log F_c \approx 1.3$ is used in Eq. (3.3) instead, these wiggles disappear. Introducing asymmetry of the broadening factors through Eq. (3.4) does practically not improve the result, see Fig. 2. Eq. (3.2) with $F_c \approx 0.37$ and $N \approx 1.3$, therefore, apparently suffices for data representation and the temperature dependence of the falloff curves is well represented in the described way. Measurements from 200 to 700 K were made in Ref. [31] for selected bath gas concentrations. The falloff curves from Fig. 3, which were constructed on the basis of the 300 K-curve alone, indeed reproduce the measured temperature dependence surprisingly well. Only the measurements near 200 K, for unknown, probably experimental, reasons, are a factor of two low.

Similar conclusions about the results near 200 K were drawn in Ref. [35]. Likewise, the fragmentary experimental data between 300 and 700 K in Ref. [35] were found to agree well with a modelled set of falloff curves. However, in the details of the modelling the present work and Ref. [35] showed differences. In particular different values of $\langle\Delta E\rangle$ and of F_c were fitted and/or modelled such that different values of $k_{-1,0}$ are obtained. For the bath gas M = He, $\langle\Delta E_{down}\rangle/hc = 200\ cm^{-1}\ (T/298\ K)^{0.1}$ was fitted in Ref. [35] which according to the relationships of Refs. [47–49] corresponds to $\beta_c(298\ K) = 0.23$ in contrast to the present value of $\beta_c = 0.1$. Comparing the derived corresponding values of $k_{-1,0}(300\ K) = [He]\ 3.16 \times 10^{-31}\ cm^6\ molecule^{-2}\ s^{-1}$ from Ref. [35] with the present value of [He] $3.96 \times 10^{-31}\ cm^6\ molecule^{-2}\ s^{-1}$, one concludes that the present modelled strong collision rate coefficient $k_{-1,0}^{SC}$ is about a factor of 3 larger than that of Ref. [35] which then is compensated by a smaller β_c. Different F_c values were also obtained in Ref. [35] and the present work. A value of $F_c = 0.54 \pm 0.01$ in Ref. [35] was fitted to the modelled results for M = He over the temperature range 200–3000 K. The present modelling led to broader weak collision falloff curves with $F_c \approx 0.37$ for M = He over the range 200–700 K. We mention these differences in the modelling details in order to illustrate typical uncertainties of the approaches. As a lot of differences compensate each other and the final results are fitted to experimental data anyway, however, they are only of small practical relevance.

4.2. Dissociation experiments

Dissociation experiments for reaction (1) are more easily done than recombination experiments for reaction (−1) and, hence, have been performed much earlier and more frequently than recombination experiments. There are secondary reactions as well, but in most cases the stoichiometry, because of fast reactions of OH with H_2O_2, was equal to 2, see Refs. [19,20]. Generally the reaction was assumed to be in the limiting low pressure range. However, this was difficult to establish experimentally such that falloff modelling is required. This is even more so, as deviations from low pressure behaviour apparently were observed in Refs. [19,20,22]. In the construction of falloff curves we again rely on calculated limiting high pressure rate coefficients such as obtained from $k_{-1,\infty}$ of Eq. (3.1) and the equilibrium constant K_c from Eqs. (2.1)–(2.3). This leads to

$$k_{1,\infty} \approx 1.05 \times 10^{15}(T/1000\ K)^{0.7}\ \exp(-E_0/RT)\ s^{-1} \quad (4.2)$$

between 700 and 1000 K and

$$k_{1,\infty} \approx 1.05 \times 10^{15}\ \exp(-E_0/RT)\ s^{-1} \quad (4.3)$$

between 1000 and 1500 K where $E_0/R = 24{,}534$ K. The falloff curves then are constructed first by assuming that the measurements at the lowest applied pressures were done at the low pressure limit and finally by adjusting the limiting low pressure rate coefficient $k_{1,0}$ according to the constructed falloff curve. By comparison with modelled strong collision values of $k_{-1,0}^{SC}$, experimental collision efficiencies β_c and average energies $\langle\Delta E\rangle$ are obtained in the end.

A series of studies with flow systems and static reactors have been performed with a variety of bath gases [13–18]. These data show an internally consistent picture, see the summaries in Refs. [8,17,18]. The most extensive measurements [17] in M = He, with bath gas pressures between 3.5 and 6.6 Torr at 919 K, and temperatures in the range 514–932 K, led to rate coefficients $k_{1,0}^{exp} = [He]\ 10^{17.35}\ \exp(-24{,}150\ K/T)\ cm^3\ mol^{-1}\ s^{-1}$. At 900 K this corresponds to $k_{1,0}^{exp} = [He]\ 5.0 \times 10^5\ cm^3\ mol^{-1}\ s^{-1}$. The modelling with a tem-

perature independent value of $-\langle\Delta E\rangle/hc = 32\ cm^{-1}$ from the analysis of the recombination experiments of Fig. 2, leads to $k_{1,0} = [He]\ 3.9 \times 10^5\ cm^3\ mol^{-1}\ s^{-1}$. The difference between the two values is well within the uncertainties of both measurements. Dissociation and recombination experiments thus appear fully consistent with each other. The construction of the falloff curve according to Section 3.3 indicates that, at the low pressures applied in Ref. [17], the measured $k_{1,0}^{exp}$ was about $0.95 \times k_{1,0}$ such that $k_{1,0} = [He]\ 5.26 \times 10^5\ cm^3\ mol^{-1}\ s^{-1}$ at 900 K and a fitted value of $-\langle\Delta E\rangle/hc = 34\ cm^{-1}$ is the final result.

Measurements with M = Ar were performed in Ref. [18], over the pressure range 15–760 Torr at 792 K, and over the temperature range 725–833 K, leading to $k_{1,0}^{exp} = [Ar]\ 10^{17.06}\ \exp(-23{,}300\ K/T)\ cm^3\ mol^{-1}\ s^{-1}$. At 800 K and 760 Torr, the measured $k_{1,0}^{exp}$ is calculated to be about 0.75 $k_{1,0}$ and $-\langle\Delta E\rangle/hc = 105\ cm^{-1}$ is the final fitted result, such as obtained analogous to the procedure described for M = He. Besides these dissociation studies with M = Ar, shock tube studies were also performed employing higher temperatures [19–24]. There was only a small temperature gap between the highest temperature (833 K) studied in Ref. [18] and the lowest temperature (950 K) of the shock tube experiments of Refs. [19,20] such that the consistency of the various techniques could be tested. A minor temperature shift between the data of Refs. [18,19] in Ref. [21] was attributed to traces of H_2O and O_2 from H_2O_2 decomposition occurring in the inlet system of those shock tube experiments. This lowers the calculated shock temperatures. After this correction was applied, the low pressure data were well consistent with each other. One should also mention that the most recent shock tube results over the pressure range 0.8–3.3 bar from Refs. [23,24] are in very good agreement with the earlier results from Refs. [19–22]. Shock wave studies with a pressure variation of about a factor of 15 were done in Refs. [19,22]. The results in Fig. 4 are compared with modelled falloff curves using the calculated $k_{1,\infty}$ and $\langle\Delta E\rangle$ derived from the analysis of $k_{1,0}^{exp}$ from Ref. [18] in the range 725–833 K, see above. The data near $[Ar] = 10^{-5}\ mol\ cm^{-3}$ (corresponding to about 1 bar) agree with the predictions, although a slightly stronger temperature dependence is predicted near to the low pressure limit. (In part this might be due to the assumption of a temperature independent $\langle\Delta E\rangle$. For our recommendations of rate coefficients, see below, we trust more on the experimental data at [Ar] near $10^{-5}\ mol\ cm^{-3}$.) With increasing pressures and temperatures, however, deviations up to about a factor of 3 are observed. At this stage no explanation for these deviations can be offered. They may be due to experimental problems, but they might also be the consequences of nonexponential lifetime distributions such as observed in the CT calculations of Ref. [33]. One therefore has to live with this uncertainty of k_1 which increases up to a factor of about 2 at temperatures above 1000 K and pressures above 10 bar. Weak collision broadening of the falloff curves for M = Ar is predicted to be slightly less pronounced than for M = He. Using the value of β_c derived from the experiments, with Eqs. (3.5) and (3.6) one obtains $F_c \approx 0.43$. Again the decrease of F_c^{WC} with increasing temperature is nearly compensated by the increase of F_c^{SC} such that F_c is nearly temperature independent. In contrast to the present work, the modelling of Ref. [35] led to $F_c = 0.55 \pm 0.01$ for M = Ar over the range 500–3000 K.

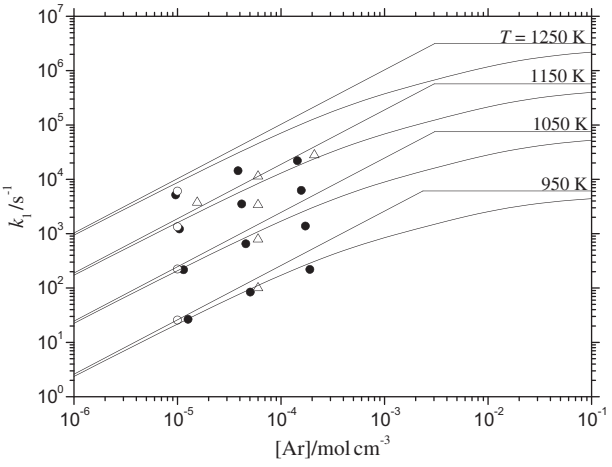

Fig. 4. Experimental dissociation rate coefficients k_1 and their modelled falloff representation (M = Ar, experimental points from Ref. [19] (△), 21 (○), and 22 (●); full lines = modelled limiting low and high pressure rate coefficients from Section 5 of this work; falloff curves = representation by Eq. (3.3) with $F_c = 0.43$ and $N = 1.22$, see text; the experimental results from Refs. [23,24] for $[Ar] = (1–5) \times 10^{-5}\ mol\ cm^{-3}$ and $T = 1000–1400$ K agree very well with the data from Ref. [22] and, for clarity, are not included in the figure).

Experiments with the bath gases M = N_2, O_2, and CO_2 near to the low pressure limit of the dissociation from Refs. [17,18,23] in the present work were also evaluated, such as described above for M = He and Ar. The resulting values for $-\langle\Delta E\rangle/hc$ are 120, 92 (averages of results based on Refs. [17,18,23]), and 117 (based only on Ref. [17]) cm^{-1} for M = N_2, O_2, and CO_2, respectively. Results for M = H_2O and H_2O_2 agree within a factor of two with modelled strong collision low pressure rate coefficients based on Lennard–Jones collision frequencies. This observation is analogous to the results for H + O_2 + M such as discussed in Ref. [45]. $k_{1,0}(H_2O)/k_{1,0}(N_2) = 4.3$ (Ref. [17]) or 6.0 (Ref. [18]) and $k_{1,0}(H_2O_2)/k_{1,0}(N_2) = 5.9$ (Ref. [17]) or 6.6 (Ref. [18]) were measured. A further analysis of these results in terms of dipole–dipole capture rate constants instead of the Lennard–Jones collision frequencies can easily be done analogous to Ref. [45]. In this case, the dipole–dipole capture rate constants are much closer to the Lennard–Jones collision frequencies (being factors of 1.18 and 0.84 different for M = H_2O and H_2O_2, respectively) than for the HO_2-system. The strong collision rate coefficients modelled with these collision frequencies are so close to the experimental results from Refs. [17,18] that weak collision effects cannot be identified ($-\langle\Delta E\rangle/hc \geqslant 1000\ cm^{-1}$).

5. Simplified representation of rate coefficients

The essential elements of our representation of the rate coefficients k_1 and k_{-1} are the limiting low and high pressure rate coefficients and the intermediate falloff expressions. In addition, k_1 and k_{-1} are linked by the equilibrium constant K_c which obviously has to be consistent with the modelling of k_1 and k_{-1}. In the following we summarize the results of the previous sections.

The equilibrium constant K_c in Section 2 was modelled with the result

$$K_c = 71.4(T/1000\ K)^{1.1} \exp(-24,534\ K/T)\ mol\ cm^{-3} \quad (5.1)$$

over the range 500–1000 K, and

$$K_c = 71.4(T/1000\ K)^{0.25} \exp(-24,534\ K/T)\ mol\ cm^{-3} \quad (5.2)$$

over the range 1000–1500 K, see Section 2. For wider temperature ranges, but less precisely, the expression $K_c = 4.23 \times 10^5\ T^{-1.066} \exp(-25{,}660\ K/T)$ was recommended in Ref. [10] over the range 300–5000 K.

The SACM-CT calculations of Ref. [33] on the ab initio potential from Ref. [32] led to the limiting high pressure rate coefficients for recombination

Table 2
Summary of recommended rate coefficients.

(a) Recombination rate coefficients (200–700 K)
$k_{-1,\infty} = 3.8 \times 10^{-10}\,(T/300\ \mathrm{K})^{-0.5}\ \mathrm{cm^3\ molecule^{-1}\ s^{-1}}$
$k_{-1,0} = [\mathrm{N_2}]\ 9.0 \times 10^{-31}\,(T/300\ \mathrm{K})^{-3.2}\ \mathrm{cm^6\ molecule^{-2}\ s^{-1}}$

(b) Dissociation rate coefficients (500–1500 K, E_0/R = 24,534 K)
$k_{1,\infty} = 1.0 \times 10^{15}\,(T/1000\ \mathrm{K})^{0.9}\ \exp(-E_0/RT)\ \mathrm{s^{-1}}$
$k_{1,0} = [\mathrm{Ar}]\ 5.2 \times 10^{-7}\,(T/1000\ \mathrm{K})^{-2.3}\ \exp(-E_0/RT)\ \mathrm{cm^3\ molecule^{-1}\ s^{-1}}$

(c) F_c = 0.37, 0.42, 0.42, 0.43, 0.43, 0.51, and 0.51 and $k_0(\mathrm{M})[\mathrm{N_2}]/k_0(\mathrm{N_2})[\mathrm{M}]$ = 0.44, 0.68, 0.79, 1.00, 1.06, 5.1, and 5.2 for M = He, Ar, O_2, N_2, CO_2, H_2O, and H_2O_2, respectively, over the range 200–1500 K

$$k_{-1,\infty} = [2.26 \times 10^{13}(298\ \mathrm{K}/T)^{0.47} + 7.83 \times 10^{11}(T/298\ \mathrm{K})^{0.74}]\ \mathrm{cm^3\ mol^{-1}\ s^{-1}} = [0.376(298\ \mathrm{K}/T)^{0.47} + 0.013(T/298\ \mathrm{K})^{0.74}] \times\ 10^{-10}\ \mathrm{cm^3\ molecule^{-1}\ s^{-1}} \quad (5.3)$$

see Section 3.1. The corresponding rate coefficient for dissociation follows by combining Eqs. (5.1) and (5.2) with Eq. (5.3). Representing the results in more compact form leads to

$$k_{1,\infty} \approx 1.04 \times 10^{15}(T/1000\ \mathrm{K})^{n} \exp(-24,534\ \mathrm{K}/T)\mathrm{s^{-1}} \quad (5.4)$$

with $n = 0.74$ over the range 600–1000 K and $n \approx 0$ over the range 1000–1500 K, while

$$k_{-1,\infty} \approx 1.48 \times 10^{13}(T/1000\ \mathrm{K})^{-0.32}\ \mathrm{cm^3\ mol^{-1}\ s^{-1}} \quad (5.5)$$

applies to the range 300–1500 K. As the available experimental falloff extrapolations to the high pressure limit apparently still have larger uncertainties than the calculations, which in turn agree well with the liquid phase results from Ref. [34], we recommend the use of calculated values of $k_{1,\infty}$ and $k_{-1,\infty}$.

The limiting low pressure rate coefficients have to be calibrated by experiments because the average energies $\langle\Delta E\rangle$ transferred per collision for the time being are fit parameters. Temperature dependences of $\langle\Delta E\rangle$ could not be identified within experimental uncertainty such that $\langle\Delta E\rangle$ as in other cases is assumed to be temperature independent. The analysis of recombination experiments suggested that $k_{-1,0}$, because of the importance of the superimposed reactions (2)–(4), could not be derived at all from Refs. [27,28]. The agreement within a factor of two of the values obtained in Refs. [27,28] with the values from the present work should rather be considered as accidental. Only by suppressing reactions (3) and (4) by adding excess O_2, in Refs. [30,31] parts of the recombination falloff curve became accessible. However, the extrapolation towards $k_{-1,0}$ was difficult. Nevertheless, the estimated $\langle\Delta E\rangle$ for M = He from the extrapolation showed agreement well with the value obtained by the analysis of high temperature dissociation experiments with M = He. $\langle\Delta E\rangle$-values for M = Ar, N_2, O_2, and CO_2 could only be obtained by analysis of dissociation experiments. On the basis of the fitted $\langle\Delta E\rangle$-values, modelled $k_{1,0}$ and $k_{-1,0}$ were calibrated. They can be represented by

$$k_{-1,0} = [\mathrm{N_2}]9.0 \times 10^{-31}(T/300\ \mathrm{K})^{-3.2}\ \mathrm{cm^6\ molecule^{-2}\ s^{-1}} = [\mathrm{N_2}]3.3 \times 10^{17}(T/300\ \mathrm{K})^{-3.2}\ \mathrm{cm^6\ molecule^{-2}\ s^{-1}} \quad (5.6)$$

This expression applies over the range 200–1000 K with an estimated uncertainty of better than a factor of two. As the temperature dependences of $k_{-1,0}$ are practically the same for many other bath gases, their $k_{-1,0}$ can be expressed by relative rate coefficients $k_{-1,0}(\mathrm{M})[\mathrm{N_2}]/k_{-1,0}(\mathrm{N_2})[\mathrm{M}]$ which, on the basis of Refs. [17,18,22–24,30] are given by 0.44, 0.68, 0.79, and 1.06 for M = He, Ar, O_2, and CO_2,respectively. For the near strong collision rate coefficients of the bath gases M = H_2O and H_2O_2, the modelling on the basis of Refs. [17,18] leads to T-exponents of −2.87 (M = H_2O) and −2.77 (M = H_2O_2) and relative rate coefficients at 300 K of 3.3 (M = H_2O) and 3.4 (M = H_2O_2).

We illustrated the differences between various levels of falloff expressions. In view of the general uncertainties, for practical applications the simple expression of Eqs. (3.2) and (3.3) should be completely sufficient to represent the pressure dependence both of k_1 and k_{-1}. The relevant center broadening factors F_c (including weak and strong collision contributions) were obtained from the modelling as $F_c \approx 0.37$ for recombination experiments in moderately weak collider bath gases like M = He and between 200 and 700 K. For dissociation experiments between 700 and 1400 K, F_c was predicted to increase to values of $F_c \approx 0.43$. The weak temperature dependence of F_c in practice appears negligible. The quality of the modelled falloff curves in Fig. 3 was illustrated where single recombination experiments near the center of the falloff curves, for M = He from Ref. [31], could well be reproduced (except at 200 K, possibly for experimental reasons). Dissociation falloff curves, near 1000 K in M = Ar, could also well be reproduced. The reasons for larger deviations from the modelled dissociation falloff curves at $T > 1100$ K could not be identified unambiguously. In practice here probably one should prefer the modelled over the experimental curves. Although details of the present modelling differ from those of the complementary modelling study of Ref. [35], the experimental data within their scatter are represented equally well. The reason for this agreement is found in different fits of the average energies transferred per collision. In order to facilitate practical applications, Table 2 summarizes the recommended rate coefficient of the present analysis. Falloff curves are represented in the simplified form of Eqs. (3.2) and (3.3) employing temperature independent F_c. High pressure rate coefficients are from the theoretical modelling of Ref. [33]. Low pressure rate coefficients are based on data from Refs. [17–29] accounting for falloff effects.

In summary, the present analysis by combination of ab initio calculations, rate modelling and limited experimental data has provided a complete set of rate coefficients for the practically very important reaction system of hydrogen peroxide dissociation and hydroxyl radical recombination.

Acknowledgments

Helpful comments on this manuscript by C.T. Bowman and K. Luther as well as technical help by A. Maergoiz and financial support by the Deutsche Forschungsgemeinschaft (TR 69/17-1) are gratefully acknowledged.

References

[1] W. Jost, Explosions- und Verbrennungsvorgänge in Gasen, Verlag J. Springer, Berlin, 1939.
[2] B. Lewis, G. von Elbe, Combustion, Flames and Explosions of Gases, third ed., Academic Press, Orlando, 1987.
[3] U. Mass, J. Warnatz, Combust. Flame 74 (1988) 53.
[4] M. O'Conaire, H.J. Curran, M.M. Simmie, W.J. Pitz, C.K. Westbrook, Int. J. Chem. Kinet. 36 (2004) 603.
[5] P. Saxena, F.A. Williams, Combust. Flame 145 (2006) 316.
[6] J. Li, Z. Zhao, A. Kazakov, M. Chaos, F.L. Dryer, J.J. Scire, Int. J. Chem. Kinet. 39 (2007) 109.
[7] C.L. Rasmussen, J. Hansen, P. Marshall, P. Glarborg, Int. J. Chem. Kinet. 40 (2008) 454.
[8] D.L. Baulch, D.D. Drysdale, D.G. Horne, A.C. Lloyd, Evaluated Kinetic Data for High Temperature Reactions, vol. 1, Butterworth, London, 1972.
[9] B. Eiteneer, M. Goldenberg, C.T. Bowman, R.K. Hanson, S. Song, W.C. Gardiner, V.V. Lissianski, Z. Qin, GRI-Mech 3.0, <http://www.me.Berkeley.edu./gri_mech/>.
[10] D.L. Baulch, C.T. Bowman, C.J. Cobos, R.A. Cox, Th. Just, J.A. Kerr, M.J. Pilling, D. Stocker, J. Troe, W. Tsang, R.W. Walker, J. Warnatz, J. Phys. Chem. Ref. Data 34 (2005) 757.
[11] R. Atkinson, D.L. Baulch, R.A. Cox, J.N. Crowley, R.F. Hampson, R.G. Hynes, M.E. Jenkin, M.J. Rossi, J. Troe, Atmos. Chem. Phys. 4 (2004) 1461.
[12] M. Thénard, Mem. Acad. Sci. (Paris) 3 (1818) 385.

[13] C.K. Mc Lane, J. Chem. Phys. 17 (1949) 379.
[14] P.A. Giguère, I.D. Liu, Can. J. Chem. 35 (1957) 283.
[15] C.N. Satterfield, T.W. Stein, J. Phys. Chem. 61 (1957) 537.
[16] W. Forst, Can. J. Chem. 36 (1958) 1308.
[17] D.E. Hoare, J.B. Protheroe, A.D. Walsh, Trans. Faraday Soc. 55 (1959) 548.
[18] R.R. Baldwin, D. Brattan, Proc. Combust. Inst. 8 (1960) 110.
[19] E. Meyer, H.A. Olschewski, J. Troe, H. Gg. Wagner, Proc. Combust. Inst. 12 (1968) 345.
[20] J. Troe, Ber. Bunsen. Phys. Chem. 73 (1969) 946.
[21] H. Kijewski, J. Troe, Helv. Chim. Acta 55 (1973) 205.
[22] Ch. Kappel, K. Luther, J. Troe, Phys. Chem. Chem. Phys. 4 (2002) 4392 (part I of this series).
[23] Z. Hong, A. Farooq, E.A. Barbour, D.F. Davidson, R.K. Hanson, J. Phys. Chem. A 113 (2009) 12919.
[24] Z. Hong, R.D. Cook, D.F. Davidson, R.K. Hanson, J. Phys. Chem. A 114 (2010) 5718.
[25] G. Black, G. Porter, Proc. R. Soc. A 266 (1962) 185.
[26] J. Caldwell, R.A. Back, Trans. Faraday Soc. 61 (1965) 1939.
[27] D.W. Trainor, C.W. von Rosenberg, J. Chem. Phys. 61 (1974) 1010.
[28] R. Zellner, F. Ewig, R. Paschke, G. Wagner, J. Phys. Chem. 92 (1988) 4184.
[29] K. Fagerstrom, A. Lund, G. Mahmound, J.T. Jodkowski, E. Ratajczak, Chem. Phys. Lett. 224 (1994) 43.
[30] R. Forster, M. Frost, D. Fulle, H.F. Hamann, H. Hippler, A. Schlepegrell, J. Troe, J. Chem. Phys. 103 (1995) 2949.
[31] D. Fulle, H.F. Hamann, H. Hippler, J. Troe, J. Chem. Phys. 105 (1996) 1001.
[32] B. Kuhn, T.R. Rizzo, D. Luckhaus, M. Quack, M. Suhm, J. Chem. Phys. 111 (1999) 2565.
[33] J. Troe, V.G. Ushakov, Phys. Chem. Chem. Phys. 10 (2008) 3915 (part II of this series).
[34] I. Janik, D.M. Bartels, C.D. Jonah, J. Phys. Chem. A 111 (2007) 1835.
[35] S.R. Sellevåg, Y. Georgievskii, J.A. Miller, J. Phys. Chem. A 113 (2009) 4457.
[36] B. Ruscic, D. Feller, D.A. Dixon, K.A. Petersen, L.B. Harding, R.L. Asher, A.F. Wagner, J. Phys. Chem. A 105 (2001) 1.
[37] J.A. Joens, J. Phys. Chem. A 105 (2001) 11041.
[38] B. Ruscic, R.E. Pinzon, M.L. Morton, N.K. Srinivasan, M.-C. Su, J.W. Sutherland, J.V. Michail, J. Phys. Chem. A 110 (2006) 6592.
[39] M.W. Chase, NIST-JANAF Thermochemical Tables, J. Phys. Chem. Ref. Data, Monograph No. 9, Woodbury, New York, 1998.
[40] L.V. Gurvich (Ed.), Thermodynamic Properties of Individual Substances, TSIV, Moscow, 1978, 1979, 1982, 1989.
[41] X. Luo, P.R. Fleming, T.R. Rizzo, J. Chem. Phys. 96 (1992) 5659.
[42] B.G. Sumpter, D.L. Thompson, J. Chem. Phys. 82 (1985) 4557.
[43] D. Luckhaus, Habilitation Thesis, ETH Zürich, 1998. (Data cited in Ref. [33]).
[44] J.V. Michael, M.-C. Su, J.W. Sutherland, J.J. Carroll, A.F. Wagner, J. Phys. Chem. A 106 (2002) 5297.
[45] R.X. Fernandes, K. Luther, J. Troe, V.G. Ushakov, Phys. Chem. Chem. Phys. 10 (2008) 4313.
[46] A.W. Jasper, S.J. Klippenstein, L.B. Harding, J. Phys. Chem. A 111 (2007) 8699.
[47] J. Troe, J. Chem. Phys. 66 (1977) 4745.
[48] J. Troe, J. Chem. Phys. 66 (1977) 4758.
[49] J. Troe, J. Phys. Chem. 83 (1979) 114.
[50] J. Troe, V.G. Ushakov, J. Phys. Chem. A 113 (2009) 3940.
[51] R.C. Reid, J.M. Prausnitz, T.K. Sherwood, The Properties of Gases and Liquids, third ed., McGraw-Hill, New York, 1977.
[52] P. Paul, J. Warnatz, Proc. Combust. Inst. 27 (1998) 495.
[53] A.I. Maergoiz, E.E. Nikitin, J. Troe, V.G. Ushakov, J. Chem. Phys. 105 (1996) 6277.
[54] R.G. Gilbert, K. Luther, J. Troe, Ber. Bunsen. Phys. Chem. 87 (1983) 169.
[55] J. Troe, Ber. Bunsen. Phys. Chem. 87 (1983) 161.
[56] J. Troe, V.G. Ushakov, Faraday Disc. 119 (2001) 145.
[57] J. Troe, V.G. Ushakov, in preparation.
[58] L.B. Harding, A.F. Wagner, Proc. Combust. Inst. 22 (1988) 983.
[59] Y. Bedjanian, G. LeBras, G. Poulet, J. Phys. Chem. A 103 (1999) 7017.
[60] H. Sun, Z. Li, Chem. Phys. Lett. 399 (2004) 33.
[61] M.S. Woolridge, R.K. Hanson, C.T. Bowman, Int. J. Chem. Kinet. 26 (1994) 389.